



Daria Khanukaeva 

# Filtration of micropolar liquid through a membrane composed of spherical cells with porous layer

Received: 28 July 2019 / Accepted: 4 April 2020 / Published online: 27 April 2020  
© Springer-Verlag GmbH Germany, part of Springer Nature 2020

**Abstract** This paper considers membranes of globular structure in the framework of the cell model technique. The flow of a micropolar fluid through a spherical cell consisting of a solid core, porous layer and liquid envelope is modeled using coupled micropolar and Brinkman-type equations. The solution is obtained in analytical form. Boundary value problems with different conditions on the hypothetical cell surface are considered and compared. The hydrodynamic permeability of the membrane is investigated as a function of micropolar and porous media characteristics.

**Keywords** Micropolar fluid flow · Cell model · Porous medium · Hydrodynamic permeability

## 1 Introduction

The majority of porous media, especially some types of membranes, can be represented as a chaotic assemblage of particles of various shapes and sizes [1, 2]. Fibrous membranes are usually modeled as a package of cylindrical fibers or cylindrical cells. Globular structures can be described by a swarm of spherical or spheroidal particles of some average size, defined by the pore size distribution.

The Happel–Brenner cell model [3] is widely used for the modeling of filtration flows in porous structures. This method is well developed for all types of geometrically symmetric cells in the case of Newtonian liquid flows [4–14]. The idea is to consider a single particle encapsulated in a hypothetical cell; the effect of neighboring particles is taken into account via boundary conditions on the cell surface. The particle can be solid, porous, or have a solid core covered by a porous layer. Alternatively, two immiscible liquids can be taken to be the core and the envelope, respectively. A cell consisting of a solid core and a porous non-deformable hydrodynamically uniform layer that simulates a partially degraded membrane was originally developed in [5]. The Stokes–Brinkman system of governing equations was solved with various types of boundary conditions on solid surfaces and the outer hypothetical cell surface, namely Happel [15, 16], Kuwabara [17], Mehta–Morse [18] or Cunningham [19], Kvashnin [20] conditions.

All the papers mentioned above have only considered Newtonian fluids, while a great number of liquids exhibit rheology and properties (especially on a microscale and in the vicinity of boundaries), which cannot be adequately described by classical models. The existence of a wide variety of non-Newtonian models confirms the fact that all of them are far from being universal, although in certain cases very good agreement with observations has been achieved. The situation is even worse with flows in porous media, as mentioned in review [21].

---

Communicated by Tim Colonius.

---

D. Khanukaeva (✉)  
Gubkin Russian State University of Oil and Gas (National Research University), Leninsky Prospect, 65-1, Moscow,  
Russia 119991  
E-mail: khanuk@yandex.ru

Filtration of liquids with microstructure has remained almost unstudied, while the theory and applications of free micropolar flows have been well developed. Media with microstructure introduced by the Cosserat brothers [22] consist of elements which can rotate independently of their translational motion. They experience stresses and couple stresses described by the nonsymmetric tensors. Therefore, such liquids are called polar or micropolar to distinguish them from Newtonian liquids, which are nonpolar media. For simple microfluids, the dependency between the deformation rate tensor and the stress tensor remains linear, in contrast to non-Newtonian models. Also, the curvature-twist rate tensor is linearly related to the couple stress tensor for simple microfluids. The mathematical theory of micropolar flows was offered by Eringen [23, 24] and has been actively developed in the last decades. The application of the micropolar fluid theory includes, but is not restricted to the flows of suspensions, lubricants, and physiological liquids such as blood and synovial liquid. Besides, many problem statements in the framework of simple microfluids allow analytical solutions both for free and for filtration flows. A review of the existing analytical solutions and basic applications of simple microfluids was made by Khanukaeva and Filippov [25]. The formulation of boundary value problems for composite cells with a solid core, porous layer and micropolar liquid layer was presented in the aforementioned review as well. The micropolar model thus seems to be very efficient for simulating dispersed media flows in porous regions.

Only few works have dealt with micropolar flows in cell models [26–29]. The problem of a flow along the axis of a composite solid–porous cylindrical cell was solved and analyzed in [30]. The perpendicular flow in a cylindrical cell of the same structure was considered by the same authors in [31]. To the best of our knowledge, a combined, solid–porous particle in a spherical cell has not been studied before. The present paper is devoted to the modeling of a micropolar liquid flow through a membrane, which is represented by a set of spherical cells. All known types of boundary conditions at the outer surface of the cell are considered and compared, as thus far none of them have turned out to be preferable over the others. An appropriate generalization of the boundary value problem for micropolar liquids is also made and discussed.

The obtained analytical solution of the problem is used for the calculation of the hydrodynamic permeability of the membrane as a whole. Owing to the explicit form of the obtained expression for the hydrodynamic permeability, its dependencies on the boundary conditions, and liquid and porous layer characteristics can be investigated in their whole ranges. However, the cumbersome representation of the expression does not allow its analytical study. Therefore, the numeric parametric investigation of the hydrodynamic permeability is performed. The results are then compared with experimental observations.

## 2 Problem statement

The cell consists of three concentric layers, as shown in Fig. 1. The solid core has radius  $a$ ; it is covered with a uniform porous layer  $a < r < b$  (Region 1), which in turn is surrounded by a free micropolar liquid layer  $b < r < c$  (Region 2). The spherical coordinate system  $(r, \theta, \varphi)$  is introduced so that the direction of uniform flow velocity vector  $\mathbf{U}$  corresponds to  $\theta = 0$ , ( $0 \leq \theta \leq \pi$ ,  $0 \leq \varphi < 2\pi$ ). The velocity magnitude is small enough for the Stokes approach to be applicable.

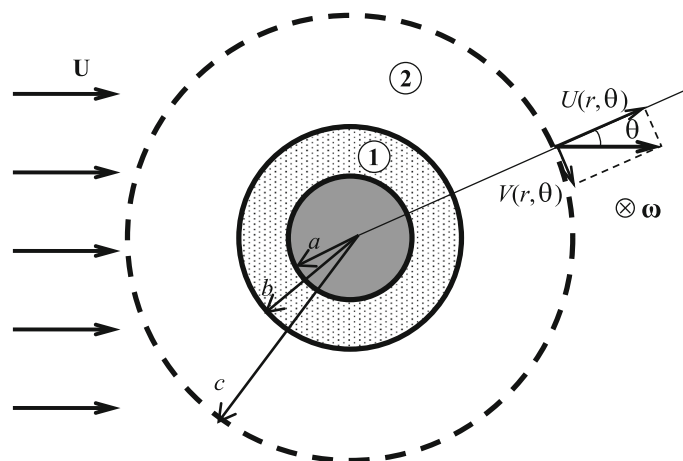


Fig. 1 Scheme of the flow

According to the theory of micropolar fluids, developed by Eringen [24,32], the steady creeping flow in Region 2 is governed by the following equations: the continuity equation, the momentum equation, and the moment of momentum equation

$$\begin{aligned}\nabla \cdot \mathbf{v} &= 0, \\ \mathbf{0} &= \rho \mathbf{F} - \nabla P + (\mu + \kappa) \Delta \mathbf{v} + 2\kappa \nabla \times \boldsymbol{\omega}, \\ \mathbf{0} &= \rho \mathbf{L} + (\alpha + \delta - \zeta) \nabla \nabla \cdot \boldsymbol{\omega} + (\delta + \zeta) \Delta \boldsymbol{\omega} + 2\kappa \nabla \times \mathbf{v} - 4\kappa \boldsymbol{\omega},\end{aligned}$$

where  $\mathbf{v}$  and  $\boldsymbol{\omega}$  are the linear velocity and the angular velocity (or spin) vectors,  $P$  is the pressure,  $\rho$  is the liquid density,  $\mathbf{F}$  and  $\mathbf{L}$  are the body force and body moment per unit mass, respectively,  $\mu$ ,  $\kappa$ ,  $\alpha$ ,  $\delta$ ,  $\zeta$  are viscosity coefficients of the micropolar medium.

Coefficient  $\mu$  is an ordinary coefficient of dynamic viscosity for the Newtonian liquid, obtained from the considered micropolar liquid in the limiting case of zero rotational viscosity  $\kappa$ . In the theory of simple microfluids, these coefficients linearly relate the stress tensor  $\hat{t}$  to the symmetric,  $\hat{\gamma}^{(S)}$  and skew symmetric,  $\hat{\gamma}^{(A)}$  parts of the deformation rate tensor  $\hat{\gamma}$ , defined as  $\hat{\gamma} = (\nabla \mathbf{v})^T - \hat{\varepsilon} \cdot \boldsymbol{\omega}$ , where  $\hat{\varepsilon}$  is the Levi-Civita tensor. The stress tensor is presented as a sum of the symmetric and skew symmetric parts, the spherical part being written separately, as is usually done in classical hydrodynamics:

$$\hat{t} = (-P + \lambda \text{tr} \hat{\gamma}) \hat{G} + 2\mu \hat{\gamma}^{(S)} + 2\kappa \hat{\gamma}^{(A)},$$

where  $\hat{G}$  is the metric tensor. One can note that  $\text{tr} \hat{\gamma} = 0$  for incompressible fluids, so consideration of the coefficient  $\lambda$  may be omitted.

Angular viscosities  $\alpha$ ,  $\delta$ ,  $\zeta$  are coefficients in the constitutive equation, respectively, relating the spherical, symmetric, and skew symmetric parts of the curvature-twist rate tensor  $\hat{\chi} = (\nabla \boldsymbol{\omega})^T$  with the couple stress tensor  $\hat{m}$ :

$$\hat{m} = \alpha (\text{tr} \hat{\chi}) \hat{G} + 2\delta \hat{\chi}^{(S)} + 2\zeta \hat{\chi}^{(A)}.$$

The chosen notation of the viscosity coefficients follows the form accepted in the micropolar theory of elasticity [33] and slightly differs from the original notation of Eringen. The only reason for this choice is the convenience in comparison with the nonpolar limiting case. The correspondence with the original notation of [24,32] can be achieved by formal re-notation.

Using the equality  $\nabla \times \nabla \times \mathbf{a} = \nabla \nabla \cdot \mathbf{a} - \Delta \mathbf{a}$ , the continuity equation, and  $\nabla \cdot \boldsymbol{\omega} = 0$ , arising from the symmetry of the cell, the governing equations for the free micropolar fluid (domain  $b < r < c$ ) in the absence of external forces and couples can be written as

$$\begin{aligned}\nabla \cdot \mathbf{v}_2 &= 0, \\ -(\mu + \kappa) \nabla \times \nabla \times \mathbf{v}_2 + 2\kappa \nabla \times \boldsymbol{\omega}_2 &= \nabla P_2, \\ -(\delta + \zeta) \nabla \times \nabla \times \boldsymbol{\omega}_2 + 2\kappa \nabla \times \mathbf{v}_2 - 4\kappa \boldsymbol{\omega}_2 &= 0,\end{aligned}\tag{1}$$

where subscript 2 corresponds to layer 2 in Fig. 1. Subscript 1 will be used for the porous Region 1, where the filtration flow occurs.

The filtration flow of micropolar liquid is governed by the Brinkman-type equations, derived by Kamel et al. [34], using the intrinsic volume averaging technique:

$$\begin{aligned}\nabla \cdot \mathbf{v} &= 0, \\ \nabla P &= \left( \frac{\mu}{\varepsilon} + \frac{\kappa}{\varepsilon} \right) \Delta \mathbf{v} + \frac{2\kappa}{\varepsilon} \nabla \times \boldsymbol{\omega} - \frac{\mu + \kappa}{k} \mathbf{v}, \\ 0 &= (\alpha + \delta - \zeta) \nabla \cdot \langle \nabla \cdot \boldsymbol{\omega} \rangle + (\delta + \zeta) \Delta \boldsymbol{\omega} + 2\kappa \nabla \times \mathbf{v} - 4\kappa \boldsymbol{\omega},\end{aligned}$$

where  $k$  is the permeability and  $\varepsilon$  is the porosity of the porous medium.  $\langle \nabla \cdot \boldsymbol{\omega} \rangle$  is the volume-averaged divergence, which can be ignored, since the spin field is divergence-free for the considered cell geometry. A detailed discussion of the filtration equations for the more general case of media with variable porosity can be found in [35].

Using the aforementioned vector equality, the governing equations for the porous region ( $a < r < b$ ) can be presented as

$$\nabla \cdot \mathbf{v}_1 = 0,$$

$$\begin{aligned} & -\left(\frac{\mu}{\varepsilon} + \frac{\kappa}{\varepsilon}\right) \nabla \times \nabla \times \mathbf{v}_1 + \frac{2\kappa}{\varepsilon} \nabla \times \boldsymbol{\omega}_1 - \frac{\mu + \kappa}{k} \mathbf{v}_1 = \nabla P_1, \\ & -(\delta + \zeta) \nabla \times \nabla \times \boldsymbol{\omega}_1 + 2\kappa \nabla \times \mathbf{v}_1 - 4\kappa \boldsymbol{\omega}_1 = 0. \end{aligned} \quad (2)$$

If the following non-dimensional variables and values are used

$$\tilde{r} = \frac{r}{b}, \quad \ell = \frac{a}{b}, \quad m = \frac{c}{b}, \quad \tilde{\mathbf{v}} = \frac{\mathbf{v}}{U}, \quad \tilde{\boldsymbol{\omega}} = \frac{\boldsymbol{\omega}b}{U}, \quad \tilde{P} = \frac{Pb}{\mu U}, \quad (3)$$

the non-dimensional forms of systems (1) and (2) will correspondingly be

$$\begin{aligned} & \tilde{\nabla} \cdot \tilde{\mathbf{v}}_2 = 0, \\ & -(\mu + \kappa) \tilde{\nabla} \times \tilde{\nabla} \times \tilde{\mathbf{v}}_2 + 2\kappa \tilde{\nabla} \times \tilde{\boldsymbol{\omega}}_2 = \mu \tilde{\nabla} \tilde{P}_2, \\ & -\frac{\delta + \zeta}{b^2} \tilde{\nabla} \times \tilde{\nabla} \times \tilde{\boldsymbol{\omega}}_2 + 2\kappa \tilde{\nabla} \times \tilde{\mathbf{v}}_2 - 4\kappa \tilde{\boldsymbol{\omega}}_2 = 0, \end{aligned} \quad (4)$$

and

$$\begin{aligned} & \tilde{\nabla} \cdot \tilde{\mathbf{v}}_1 = 0, \\ & -\frac{\mu + \kappa}{\varepsilon} \tilde{\nabla} \times \tilde{\nabla} \times \tilde{\mathbf{v}}_1 + \frac{2\kappa}{\varepsilon} \tilde{\nabla} \times \tilde{\boldsymbol{\omega}}_1 - \frac{\mu + \kappa}{k} b^2 \tilde{\mathbf{v}}_1 = \mu \tilde{\nabla} \tilde{P}_1, \\ & -\frac{\delta + \zeta}{b^2} \tilde{\nabla} \times \tilde{\nabla} \times \tilde{\boldsymbol{\omega}}_1 + 2\kappa \tilde{\nabla} \times \tilde{\mathbf{v}}_1 - 4\kappa \tilde{\boldsymbol{\omega}}_1 = 0. \end{aligned} \quad (5)$$

Systems (4) and (5) contain several dimensional constants, which can be combined in three non-dimensional parameters. The dimensions of the viscosities  $\mu$  and  $\kappa$  are the same, so the parameter  $N^2 = \kappa/(\mu + \kappa)$  introduced in [36] is non-dimensional and is called the micropolarity number or the coupling number. Another non-dimensional parameter of the micropolar liquid is the scale factor  $L^2 = \frac{\delta + \zeta}{4\mu b^2}$  [36], which represents the relation between the microscale of the problem,  $(\delta + \zeta)/\mu$ , and the macroscale,  $b$ . The third parameter,  $\sigma = b/\sqrt{k}$ , characterizes the specifics of the filtration part of the flow. It represents the ratio of the macroscale of the cell,  $b$ , to the microscale of the porous layer,  $\sqrt{k}$ . With these three non-dimensional parameters introduced, systems (4) and (5) take the following form (tildes are omitted here and hereafter):

$$\begin{aligned} & \nabla \cdot \mathbf{v}_2 = 0, \\ & -\frac{1}{N^2} \nabla \times \nabla \times \mathbf{v}_2 + 2\nabla \times \boldsymbol{\omega}_2 = \left(\frac{1}{N^2} - 1\right) \nabla P_2, \\ & -L^2 \nabla \times \nabla \times \boldsymbol{\omega}_2 + \frac{1}{2} \frac{N^2}{1 - N^2} \nabla \times \mathbf{v}_2 - \frac{N^2}{1 - N^2} \boldsymbol{\omega}_2 = 0, \end{aligned} \quad (6)$$

and

$$\begin{aligned} & \nabla \cdot \mathbf{v}_1 = 0, \\ & -\frac{1}{N^2} \nabla \times \nabla \times \mathbf{v}_1 + 2\nabla \times \boldsymbol{\omega}_1 - \frac{\varepsilon \sigma^2}{N^2} \mathbf{v}_1 = \varepsilon \left(\frac{1}{N^2} - 1\right) \nabla P_1, \\ & -L^2 \nabla \times \nabla \times \boldsymbol{\omega}_1 + \frac{1}{2} \frac{N^2}{1 - N^2} \nabla \times \mathbf{v}_1 - \frac{N^2}{1 - N^2} \boldsymbol{\omega}_1 = 0. \end{aligned} \quad (7)$$

The symmetry of the flow allows us to obtain general solutions of systems (6) and (7) in the form  $\mathbf{v}_i(r, \theta) = \{u_i(r) \cos \theta; v_i(r) \sin \theta; 0\}$ ,  $\boldsymbol{\omega}_i(r, \theta) = \{0; 0; \omega_i(r) \sin \theta\}$ ,  $P_i(r, \theta) = p_i(r) \cos \theta$ ,  $i = 1, 2$ . Both system (6) and system (7) reduce to scalar differential equations, requiring twelve conditions for the correct statement of the boundary value problem (BVP).

The no-slip and no-spin conditions on all solid surfaces were essential in the derivation of filtration Eq. (2) in [34]. So, it is necessary to set these conditions on the boundary  $r = \ell$ :

$$u_1(\ell) = 0, \quad v_1(\ell) = 0, \quad \omega_1(\ell) = 0. \quad (8)$$

Among a variety of conditions at the liquid–porous interface, the most natural (from the mechanical point of view) is the continuity of all linear and angular velocity components, i.e.,

$$u_1(1-0) = u_2(1+0), \quad v_1(1-0) = v_2(1+0), \quad \omega_1(1-0) = \omega_2(1+0). \quad (9)$$

Besides, the continuity of the stress and couple stress tensor components, normal and tangential to the surface  $r = 1$ , is adopted in this study. The corresponding components of the stress and couple stress tensors in the micropolar liquid for the chosen coordinate system are

$$\begin{aligned} t_{rr} &= (-p(r) + 2\mu u'(r)) \cos \theta, \\ t_{r\theta} &= \left( (\mu + \kappa)v'(r) - (\mu - \kappa)\frac{u(r) + v(r)}{r} - 2\kappa\omega(r) \right) \sin \theta, \\ m_{r\phi} &= \left( (\delta + \zeta)\omega'(r) - (\delta - \zeta)\frac{\omega(r)}{r} \right) \sin \theta. \end{aligned}$$

The derivation of the filtration equations for micropolar liquids [34] demonstrated that all viscous terms have coefficients equal to the viscosities of a pure liquid divided by the porosity. So, along with the effective viscosity,  $\mu/\varepsilon$ , used in the filtration models of Newtonian liquids,  $\kappa/\varepsilon$ ,  $\delta/\varepsilon$ , and  $\zeta/\varepsilon$  are to be used instead of  $\mu$ ,  $\kappa$ ,  $\delta$ ,  $\zeta$  in the expressions for the stress and couple stress tensor components in the porous region. If relations (3) are applied, the boundary conditions for stresses and couple stresses will take the following non-dimensional form:

$$-p_1(1-0) + \frac{2}{\varepsilon}u'_1(1-0) = -p_2(1+0) + 2u'_2(1+0), \quad (10)$$

$$\begin{aligned} \frac{1}{\varepsilon}v'_1(1-0) - \frac{1-2N^2}{\varepsilon}\frac{u_1(1-0) + v_1(1-0)}{1-0} - 2\frac{N^2}{\varepsilon}\omega_1(1-0) \\ = v'_2(1+0) - (1-2N^2)\frac{u_2(1+0) + v_2(1+0)}{1+0} - 2N^2\omega_2(1+0), \end{aligned} \quad (11)$$

$$\frac{1}{\varepsilon}\omega'_1(1-0) - \frac{\phi}{\varepsilon}\frac{\omega_1(1-0)}{1-0} = \omega'_2(1+0) - \phi\frac{\omega_2(1+0)}{1+0}, \quad (12)$$

with an additional non-dimensional parameter,  $\phi = (\delta - \zeta)/(\delta + \zeta)$ , introduced in Eq. (12). Due to the non-symmetry of the couple stress tensor, viscosities  $\delta$  and  $\zeta$  entered this condition independently and cannot be reduced to the parameters  $N$  and  $L$ . It is worth noting that the parameter  $\phi$  arises in the problem for a flow along the axis of a cylindrical cell [30] and does not appear in the case of a flow directed perpendicular to the cell axis [31]. So, the non-symmetric properties that the micropolar liquid exhibits at the boundary are substantially predefined by the geometry of the flow. The variation interval of  $\phi$  is  $[-1; 1]$ , the case of  $\phi = 0$  ( $\delta = \zeta$ ) being important, as it implies the absence of an explicit dependence of the solution on  $\delta$  and  $\zeta$ .

Three more boundary conditions should be set at the surface  $r = m$ . The first of them is the standard continuity condition for the normal component of the linear velocity:

$$u_2(m) = 1. \quad (13)$$

As the second condition at the outer boundary of the cell, four types of conditions known in classical cell models for Newtonian liquids will be used. They are:

Happel's no-stress condition [15],  $t_{r\theta}|_{r=m} = 0$ :

$$v'_2(m-0) - (1-2N^2)\frac{u_2(m-0) + v_2(m-0)}{m-0} - 2N^2\omega_2(m-0) = 0, \quad (14a)$$

Kuwabara's vorticity-free condition [17],  $\text{curl } \mathbf{v}_2(r, \theta)|_{r=m} = 0$ :

$$v'_2(m-0) + \frac{u_2(m-0) + v_2(m-0)}{m-0} = 0, \quad (14b)$$

the symmetry of the velocity profile by Kvashnin [20]

$$v'_2(m-0) = 0, \quad (14c)$$

and the condition of the flow uniformity by Cunningham [19]

$$v_2(m-0) = -1. \quad (14d)$$

The third condition at  $r = m$  should deal with microrotation or couple stresses. This could be a Happel-type no-couple stress condition  $m_r \varphi|_{r=m} = 0$ :

$$\omega_2'(m-0) - \phi \frac{\omega_2(m-0)}{m-0} = 0, \quad (15a)$$

the no-spin condition, which can be regarded as a Kuwabara-type or a Cunningham-type condition:

$$\omega_2(m-0) = 0, \quad (15b)$$

or a Kvashnin-type symmetry of the spin profile:

$$\omega_2'(m-0) = 0. \quad (15c)$$

Various types of slips, say,  $\omega_2(m) - \beta \omega_2'(m) = 0$  or  $\omega_2(r)|_{r=m} = n \operatorname{curl} \mathbf{v}_2(r)|_{r=m}$  with parameters  $\beta$  and  $n$ , can also be taken as the boundary conditions. Some of them are discussed in [25] and references therein. One of the recent works, dealing with slip conditions both for linear velocity and for microrotation, is [37].

Two BVPs for a flow along and across the axis of the cylindrical cell with Happel's no-stress condition and conditions (15a) or (15b) were considered and compared in [30,31]. Conditions (15a) and (15c) coincide for the flow perpendicular to the axis of the cylindrical cell. Both investigations showed that the influence of different boundary conditions (15a–15c) on the solution was rather small. The difference of a few percent was obtained for the hydrodynamic permeability of the membrane, calculated using the two aforementioned BVP solutions. Therefore, the present work is focused on the comparison of the BVP solutions with boundary conditions (14a–14d), and condition (15a) is taken as the closing one.

### 3 General solution of the problem

The solution of systems (6) and (7) was obtained purely analytically using the following procedure. The curl operator applied to the momentum equation in system (6) gives

$$\nabla \times \nabla \times \boldsymbol{\omega}_2 = \frac{1}{2N^2} \nabla \times \nabla \times \nabla \times \mathbf{v}_2. \quad (16)$$

Substituting this relation in the moment of momentum equation of system (6) results in the following expression for  $\boldsymbol{\omega}_2$

$$\boldsymbol{\omega}_2 = \frac{1}{2} \nabla \times \mathbf{v}_2 - \frac{L^2}{2N^2} \left( \frac{1}{N^2} - 1 \right) \nabla \times \nabla \times \nabla \times \mathbf{v}_2. \quad (17)$$

Expression (17), substituted into Eq. (16), reduces it to

$$\nabla \times \nabla \times \mathbf{z}_2 + \frac{N^2}{L^2} \mathbf{z}_2 = \mathbf{0}, \quad (18)$$

where  $\mathbf{z}_2 = \nabla \times \nabla \times \nabla \times \mathbf{v}_2$ . Due to the symmetry of the flow, which allowed separation of variables for all the unknown functions, such separation can also be done for  $\nabla \times \mathbf{v}_2$  and  $\mathbf{z}_2$ . For  $\nabla \times \mathbf{v}_2$ , it looks like  $\nabla \times \mathbf{v}_2 = \{0; 0; y_2(r) \sin \theta\}$ , where

$$y_2(r) = v_2'(r) + \frac{u_2(r) + v_2(r)}{r}; \quad (19)$$

for  $\mathbf{z}_2$  it reads  $\mathbf{z}_2 = \{0; 0; z_2(r) \sin \theta\}$ , where

$$z_2(r) = -y_2''(r) - \frac{2y_2'(r)}{r} + \frac{2y_2(r)}{r^2}. \quad (20)$$

Separation of variables in Eq. (18) gives the modified Bessel equation  $z_2'' + 2\frac{z_2'}{r} - z_2\left(\frac{2}{r^2} + \frac{N^2}{L^2}\right) = 0$ . Its solution is  $z_2(r) = (\tilde{C}_1 I_{3/2}(Nr/L) + \tilde{C}_2 K_{3/2}(Nr/L))/\sqrt{r}$ , where  $I_{3/2}(\xi)$ ,  $K_{3/2}(\xi)$  are, respectively, the modified Bessel and Macdonald functions of the order 3/2, and  $\tilde{C}_1$ ,  $\tilde{C}_2$  are arbitrary constants. Solving Eq. (20) with the given function  $z_2(r)$  yields  $y_2(r)$ . The continuity equation combined with Eq. (19) with the substituted  $y_2(r)$  allows us to find both linear velocity components:

$$\begin{aligned} u_2(r) &= \frac{C_1}{r^3} + \frac{C_2}{r} + C_3 + C_4 r^2 + \frac{C_5}{r^{3/2}} I_{3/2}\left(\frac{N}{L}r\right) + \frac{C_6}{r^{3/2}} K_{3/2}\left(\frac{N}{L}r\right), \\ v_2(r) &= -r u_2'(r)/2 - u_2(r). \end{aligned}$$

The angular velocity component is obtained from relation (17) as follows:

$$\omega_2(r) = \frac{C_2}{2r^2} - \frac{5}{2}C_4 r - \frac{C_5}{4L^2\sqrt{r}} I_{3/2}\left(\frac{N}{L}r\right) - \frac{C_6}{4L^2\sqrt{r}} K_{3/2}\left(\frac{N}{L}r\right).$$

The presence of an additional member in the momentum equation of system (7) induces modifications in the method of its solution. Applying the same procedure, we arrive at the equation for  $\nabla \times \mathbf{v}_1$ , which cannot be reduced to the equation for  $\nabla \times \nabla \times \nabla \times \mathbf{v}_1$  and looks like

$$\nabla \times \nabla \times \nabla \times \nabla \times \nabla \times \mathbf{v}_1 + \left(\frac{N^2}{L^2} + \varepsilon\sigma^2\right) \nabla \times \nabla \times \nabla \times \mathbf{v}_1 + \frac{\varepsilon\sigma^2 N^2}{(1-N^2)L^2} \nabla \times \mathbf{v}_1 = \mathbf{0}.$$

Nevertheless, it allows for separation of variables, which leads to

$$y_1^{(IV)} + \frac{4y_1'''}{r} - \frac{4y_1''}{r^2} - \left(\frac{N^2}{L^2} + \varepsilon\sigma^2\right) \left(y_1'' + \frac{2y_1'}{r} - \frac{2y_1}{r^2}\right) + \frac{\varepsilon\sigma^2 N^2}{(1-N^2)L^2} y_1 = 0, \quad (21)$$

where  $y_1(r)$  is defined analogously to  $y_2(r)$ .

Equation (21) presented as  $y_1^{(IV)} + \frac{4y_1'''}{r} - \frac{4y_1''}{r^2} - (\alpha_1^2 + \alpha_2^2) \left(y_1'' + \frac{2y_1'}{r} - \frac{2y_1}{r^2}\right) + \alpha_1^2 \alpha_2^2 y_1 = 0$ , where constants  $\alpha_1$ ,  $\alpha_2$  that satisfy the system  $\begin{cases} \alpha_1^2 + \alpha_2^2 = \frac{N^2}{L^2} + \varepsilon\sigma^2, \\ \alpha_1^2 \alpha_2^2 = \frac{\varepsilon\sigma^2 N^2}{(1-N^2)L^2} \end{cases}$  can be replaced by the Bessel equation  $z_1'' + 2\frac{z_1'}{r} - z_1\left(\frac{2}{r^2} + \alpha_2^2\right) = 0$ , where  $z_1 = y_1'' + 2\frac{y_1'}{r} - y_1\left(\frac{2}{r^2} + \alpha_2^2\right)$ . Solving these two equations one after another, we get  $y_1(r) = (\tilde{C}_7 I_{3/2}(\alpha_1 r) + \tilde{C}_8 K_{3/2}(\alpha_1 r) + \tilde{C}_9 I_{3/2}(\alpha_2 r) + \tilde{C}_{10} K_{3/2}(\alpha_2 r))/\sqrt{r}$ , where  $\tilde{C}_7$ ,  $\tilde{C}_8$ ,  $\tilde{C}_9$ ,  $\tilde{C}_{10}$  are arbitrary constants.

The linear and angular velocity components for Region 1 are then found analogously to the corresponding functions in Region 2, namely

$$\begin{aligned} u_1(r) &= \frac{C_7}{r^3} + C_8 + C_9 \frac{I_{3/2}(\alpha_1 r)}{r^{3/2}} + C_{10} \frac{K_{3/2}(\alpha_1 r)}{r^{3/2}} + C_{11} \frac{I_{3/2}(\alpha_2 r)}{r^{3/2}} + C_{12} \frac{K_{3/2}(\alpha_2 r)}{r^{3/2}}, \\ v_1(r) &= -r u_1'(r)/2 - u_1(r), \\ \omega_1(r) &= -\frac{\alpha_1^2}{4N^2} \left(1 + \alpha_2^2 L^2 \left(1 - \frac{1}{N^2}\right)\right) \left(C_9 \frac{I_{3/2}(\alpha_1 r)}{\sqrt{r}} + C_{10} \frac{K_{3/2}(\alpha_1 r)}{\sqrt{r}}\right) \\ &\quad - \frac{\alpha_2^2}{4N^2} \left(1 + \alpha_1^2 L^2 \left(1 - \frac{1}{N^2}\right)\right) \left(C_{11} \frac{I_{3/2}(\alpha_2 r)}{\sqrt{r}} + C_{12} \frac{K_{3/2}(\alpha_2 r)}{\sqrt{r}}\right), \end{aligned}$$

$\theta$ -projections of the equations of motion in systems (6) and (7) give the expressions for  $p_2(r)$  and  $p_1(r)$  correspondingly.

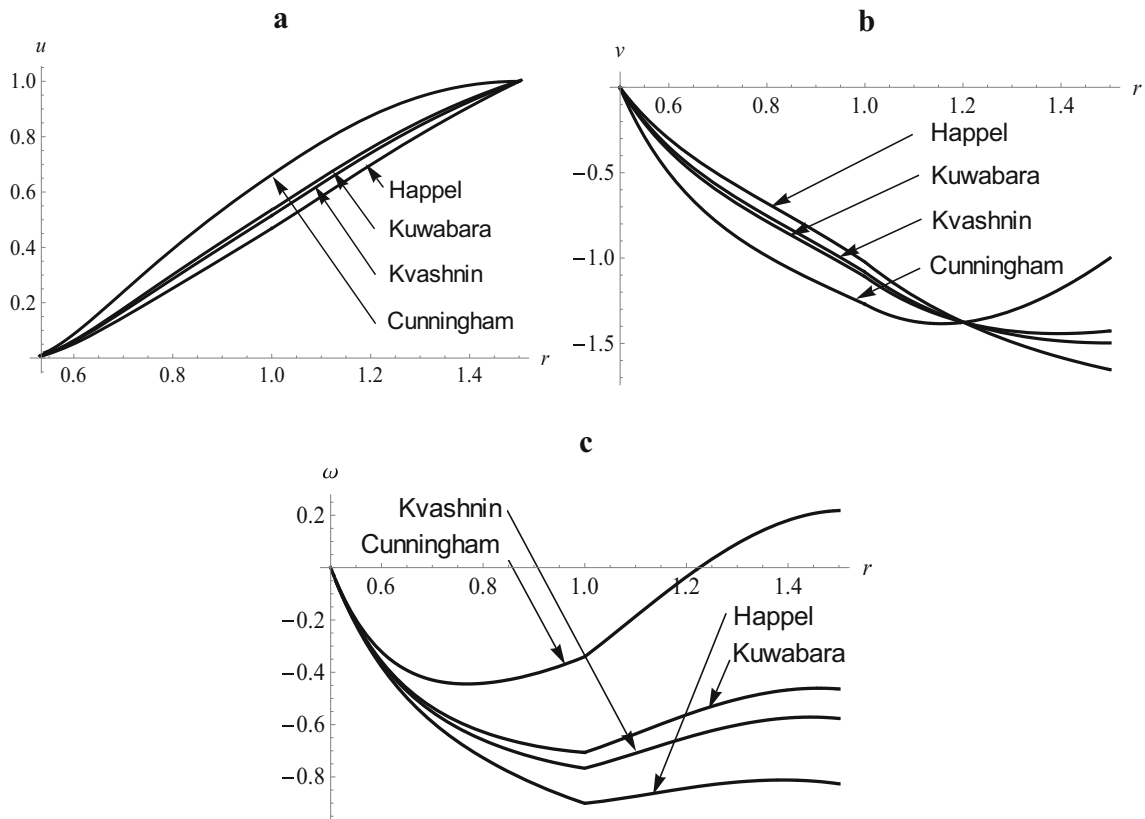


**Fig. 2** **a** Radial velocity component,  $u_i(r)$ ; **b** tangential velocity component,  $v_i(r)$ ; **c** microrotation,  $\omega_i(r)$  for BVPs with conditions (14a–14d)

#### 4 Solution of the boundary value problems

The profiles of all linear and angular velocity components as functions of  $r$  for  $\theta = 0$  are shown in Fig. 2 for the obtained solutions with conditions (8–14) and (15a) imposed. All of the curves in Fig. 2 are plotted in non-dimensional units (3) for the following values of parameters:  $\ell = 0.5$ ,  $m = 1.5$ ,  $N = 0.5$ ,  $L = 0.2$ ,  $\phi = 0.5$ ,  $\varepsilon = 0.75$ , and  $\sigma = 3$ . These values will also be used in the investigation of hydrodynamic permeability.

$\ell = 0.5$ ,  $m = 1.5$  correspond to the equal thicknesses of the porous and liquid layers, since the porous-liquid interface is located at  $r = 1$ . The thickness of the porous layer,  $1 - \ell$ , and the thickness of the solid layer,  $\ell$ , are taken to be equal to each other in order to capture the influence of both. The position of the outer cell surface corresponds to a liquid layer of the same thickness. It allows us to obtain a more or less pronounced dependence of the solution on the conditions at the outer cell surface. The higher the values of  $m$ , the further the problem is shifted to the limiting case of a singular sphere in a uniform flow.

The chosen parameters of the micropolar liquid  $N = 0.5$ ,  $L = 0.2$ ,  $\phi = 0.5$  correspond to well-developed micropolarity properties. As the coupling number  $N$  represents a fraction of the rotational viscosity in the sum of the dynamic and rotational viscosity, the range of its possible values is  $[0; 1)$ . So, the chosen value of 0.5 corresponds to one and the same order of magnitude for these coefficients, i.e., to a noticeable influence of the microrotational properties of the medium and the skew symmetric part of the stress tensor. The scale factor  $L$  contains the characteristic scale of the problem,  $b$ , along with the viscosity coefficients. The presence of the macroscopic scale in the solution deprives it of the similarity property, and this fact makes micropolar fluids principally different from the Newtonian ones. Even though the range of possible values for  $L$  is  $[0; +\infty)$ , very high values of this parameter may have no physical sense. For example,  $L > 1$  may be treated as a liquid with structural elements of the order of the whole flow region. On the other hand, one cannot interpret parameter  $L$  literally as the ratio of the micro- and macroscales of the problem, since no particles are physically present in the micropolar liquid. Figure 2 is plotted with  $L = 0.2$ , which is one of the most reasonable average



values for this parameter. The chosen value of  $\phi = 0.5$  is far from its possible limiting values, so it allows taking into account the non-symmetry of the couple stress tensor and clarifying its influence on the solution.

Medium values of  $\varepsilon = 0.75$  and  $\sigma = 3$  are characteristic of a porous medium with neutral properties. It is worth mentioning that the Brinkman equation has been derived for the case of highly porous media ( $\varepsilon > 0.6$ ), so low porosity values are not allowed for its application. Parameter  $\sigma$  relates the size of the cell core,  $b$ , and the so-called Brinkman radius,  $\sqrt{k}$ . The latter may be interpreted as the characteristic scale of the filtration flow. Thus, low values of  $\sigma$  correspond to a porous layer almost transparent for the flow. High values of  $\sigma$  are attributed to an impermeable porous layer. The chosen value of this parameter is far from both these limiting cases and is associated with a well-developed filtration flow in the porous layer of the cell.

As one can see, the differences in the boundary conditions (14a–14d) relatively weakly affect the radial velocity component and substantially influence the variation in the microrotation velocity (Fig. 2c); for the Cunningham condition, even the direction of microrotation changes. Anyway, this effect will not arise for sufficiently high values of  $m$ , i.e., for thick liquid layers.

The most interesting feature of the velocity profiles concerns the behavior of the tangential component (Fig. 2b): all the curves have one mutual intersection point. This fact implies the existence of some spherical surface approximately in the middle of the cell liquid layer, where the tangential velocity component of the flow has one and the same value for all conditions at the outer boundary. Moreover, this property holds for any values of all the parameters, both geometrical and mechanical. It is also true for Newtonian liquids and simple solid–liquid cells without a porous layer. The position of the intersection point only depends on the geometrical characteristics of the cell.

Another peculiarity of the presented velocity profiles is the corner points in Fig. 2c. These jumps of the microrotation velocity derivatives follow from the difference between the viscosity coefficients for the free micropolar liquid and the corresponding effective viscosities in the porous region. They differ by a factor of  $\varepsilon$ . Another parameter responsible for this effect is the non-symmetry of the couple stress tensor, expressed by the coefficient  $\phi$ . In the particular case of  $\varepsilon = 1$ ,  $\phi = 0$ , all microrotation velocity curves will be smooth; for the micropolar liquid with arbitrary properties this will not be the case.

## 5 Results and discussion

The proposed model and the obtained solution allow for an investigation of the membrane hydrodynamic permeability  $L_{11}$ , which is important for applications. This coefficient is defined as  $L_{11} = \frac{U}{F/V}$ , where the denominator represents the cell pressure gradient,  $F$  is the force that the flow exerts on the particle,  $V = \frac{4}{3}\pi c^3$  is the volume of the cell. The integration of the stresses over the outer surface of the porous layer yields the force  $F$

$$F = \iint_S (t_{rr} \cos \theta - t_{r\theta} \sin \theta) ds.$$

The hydrodynamic permeability takes the following non-dimensional form:

$$\begin{aligned} L_{11} &= \frac{4\pi m^3/3}{2\pi \int_0^\pi \left( [-p_2 + 2u'_2] \cos^2 \theta - \frac{1}{1-N^2} [v'_2 - (1 - 2N^2)\frac{u_2+v_2}{r} - 2N^2\omega_2] \sin^2 \theta \right) \sin \theta d\theta} \\ &= -\frac{m^3}{3C_2}. \end{aligned}$$

The results of the parametric study for  $L_{11}$  are presented below in a graphical form. The hydrodynamic permeability depends on six parameters: three characteristics of the micropolar liquid, two characteristics of the porous layer, and one characteristic of the cell geometry, called active porosity, i.e., the porosity of the membrane as a whole. Each plot shows the dependence of  $L_{11}$  on one of the listed parameters for all the four considered BVPs.

Figure 3 demonstrates the dependence of  $L_{11}$  on the micropolarity number  $N$ . One can see a substantial difference between the curves, corresponding to the BVPs with Happel's, Kuwabara's, Kvashnin's, and Cunningham's conditions. This result is non-trivial, as the differences between the velocity components shown in Fig. 2 are rather small, so one would expect an additional smoothing effect of the boundary conditions on such

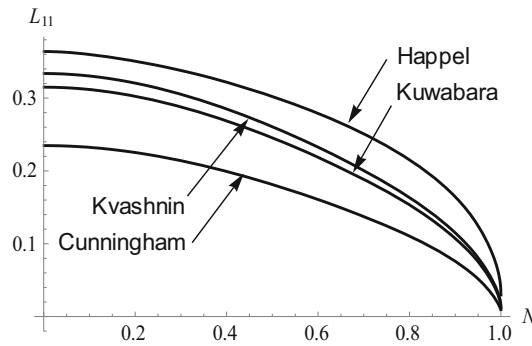


**Fig. 3** Variation in hydrodynamic permeability with coupling parameter  $N$  for different BVPs

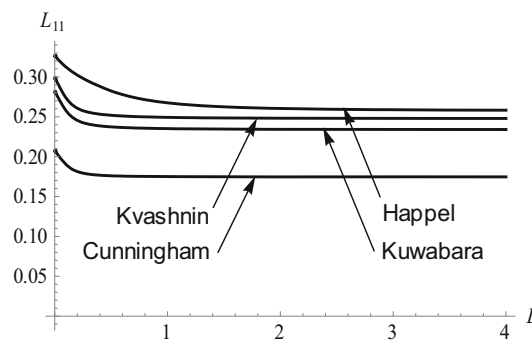


**Fig. 4** Variation in hydrodynamic permeability with scale parameter  $L$  for different BVPs

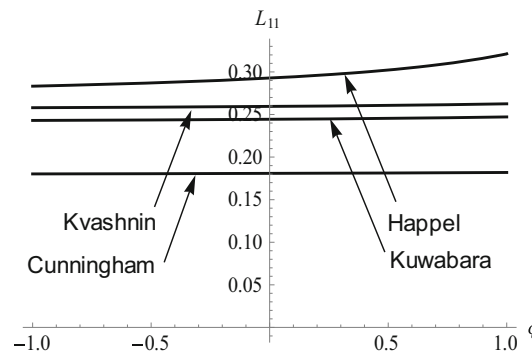


**Fig. 5** Variation in hydrodynamic permeability with parameter  $\phi$  for different BVPs

integral characteristics of the flow as  $L_{11}$ . Besides, it follows from Fig. 3 that the hydrodynamic permeability is rather sensitive to the variation in  $N$ . Maximal values of  $L_{11}$  are reached at  $N \rightarrow 0$  and correspond to the nonpolar limit, investigated in [11]. The increase in  $N$  implies the intensification of the microrotational effects and the growth of the microrotational viscosity. It leads, in turn, to higher values of the drag force and, consequently, to the diminishing of  $L_{11}$ . Nevertheless, the limiting case of  $N = 1$  cannot be reached physically.

Figure 4 depicts hydrodynamic permeability versus the scale parameter  $L$ . A clear difference in the values of  $L_{11}(L)$  is again observed for the considered BVPs. Meanwhile, the relative variation of the hydrodynamic permeability for each BVP does not exceed 25%.  $L_{11}$  reaches its maximum value at  $L = 0$ , where the effect of the angular viscosities of the liquid vanishes. With the growth of  $L$ , the influence of the liquid microstructure increases and the value of  $L_{11}$  diminishes, the character of this behavior being independent of the considered types of BVPs. The peculiarity of all the plots for  $L_{11}(L)$  is the existence of the asymptotes at  $L \rightarrow \infty$ . As seen in Fig. 4, the curves reach their asymptotic values so quickly that the magnitudes of the scale factor  $L \sim 1 \div 3$  can be treated as infinite. The asymptotical values of  $L_{11}$  are defined by the magnitude of parameter  $N$ .

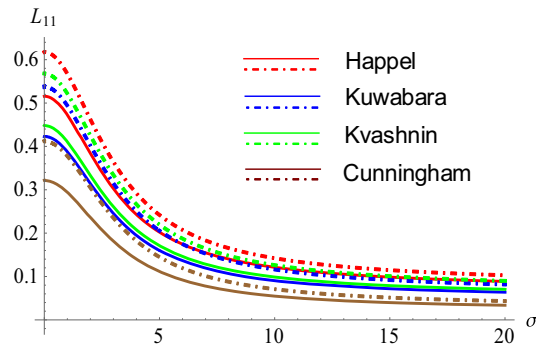


**Fig. 6** Variation in hydrodynamic permeability with parameter  $\sigma$  for different BVPs in micropolar liquid (solid lines) and in Newtonian liquid (dot-dashed lines)

The influence of the third parameter of the micropolar liquid,  $\phi$ , on the hydrodynamic permeability is shown in Fig. 5. This parameter appears in two boundary conditions for Happel's BVP and in one boundary condition in each of the remaining BVPs. As a result, it most noticeably disturbs the behavior of  $L_{11}$  for Happel's statement of the problem. For three other BVPs,  $L_{11}(\phi)$  hardly deviates from a constant value, as seen in Fig. 5. For Happel's BVP, the total variation in  $L_{11}(\phi)$  values is about 10% of its average value. Thus, in comparison with the influence of parameters  $N$  and  $L$  on the hydrodynamic permeability, the effect of  $\phi$  is almost negligible. It means that the asymmetric properties of the micropolar liquid are not crucial for the evaluation of such integral characteristics of the flow through the membrane, as  $L_{11}$ .

By definition, the permeability parameter  $\sigma$  is inversely proportional to the permeability coefficient of the porous medium of the cell. So, the higher the value of  $\sigma$ , the lower the hydrodynamic permeability of the membrane, as confirmed in Fig. 6. The values of  $\sigma$  less than unity correspond to such a highly permeable porous layer that its presence can be neglected and the flow can be considered as totally liquid in the domain of  $\ell < r < m$ . Consequently, the highest values of  $L_{11}$  are observed for all the considered BVP statements in this case. For higher values of parameter  $\sigma$ , its inverse magnitude can be treated as a fraction of the porous layer, where the major part of the filtration flow takes place. The thinner this layer, the lower the hydrodynamic permeability; in the limiting case, the flow region will be reduced to the liquid layer  $1 < r < m$ . Thus, the most complicated case of fully developed filtration in the porous layer corresponds to the values of  $\sigma \sim 1 \div 10$ . The difference in the hydrodynamic permeability corresponding to the micropolar and classical liquid models is seen in this interval. The curves plotted for the same four types of BVP in the framework of the Newtonian liquid model are shown in Fig. 6 with the dot-dashed lines. They demonstrate the dependence of  $L_{11}(\sigma)$ , analogous to that of the micropolar model, and confirm the results obtained in [11]. For each of the considered BVPs, the curve for the Newtonian liquid is located higher than the corresponding curve for the micropolar liquid. This is a natural consequence of the presence of additional degrees of freedom and viscosities in the micropolar liquid, which leads to lower values of flow velocity and hydrodynamic permeability. Nevertheless, it is worth paying attention to the position of the plot for Cunningham's model for the Newtonian liquid. Naturally, it is located lower than the curves for the other BVPs. Besides, it lies lower than the curves for the other BVPs for the micropolar liquid. This circumstance somewhat separates Cunningham's condition from the rest.

The porosity  $\varepsilon$  of the layer  $\ell < r < 1$  is an intrinsic property of the cell, which is weakly related to the apparent porosity of the membrane as a whole and can hardly be measured in an experiment. The model of a complex porous membrane, developed in the present study, is aimed at the simulation of a partially degraded membrane. The solid matrix of such membranes is covered with a partially permeable gel layer which can be considered to be a porous Brinkman-type medium [38] with the porosity  $\varepsilon$ . Anyway, this parameter significantly influences the hydrodynamic permeability of a membrane, as shown in Fig. 7. The whole range of the parameter  $\varepsilon$  variation corresponds to an approximately threefold growth of  $L_{11}$ , for both liquid models and for all types of BVPs. Nevertheless, this conclusion should be treated with caution, as the Brinkman-type model was originally designed only for the highly porous media. Similar to the dependence of  $L_{11}(\sigma)$ , the curve  $L_{11}(\varepsilon)$  for Cunningham's model in Newtonian liquid demonstrates values lower than for some BVPs for the micropolar liquid.

The active porosity of the membrane as a whole,  $\gamma$ , is usually measured in experiments. It is defined as the fraction of voids filled with liquid. In the original Happel and Brenner cell models which only included

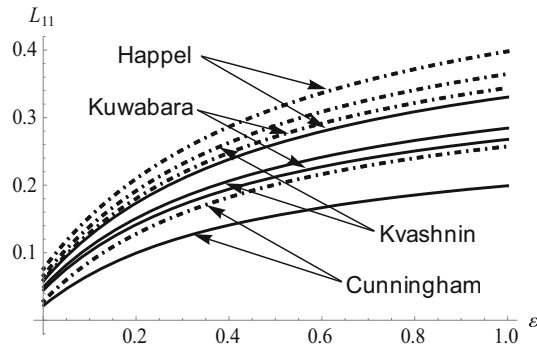


**Fig. 7** Variation in hydrodynamic permeability with porosity  $\varepsilon$  for different BVPs in micropolar liquid (solid lines) and in Newtonian liquid (dot-dashed lines)

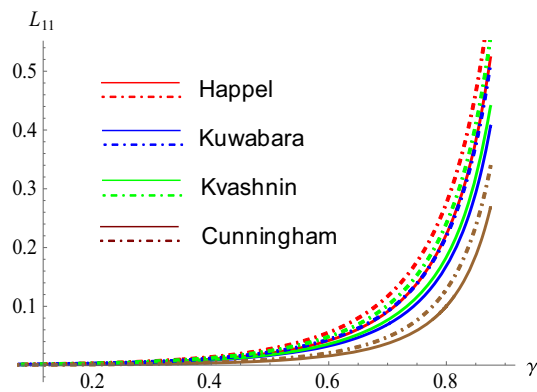


**Fig. 8** Variation in hydrodynamic permeability with porosity  $\gamma$  for different BVPs in micropolar liquid (solid lines) and in Newtonian liquid (dot-dashed lines)

the solid core of radius  $b$  and the liquid shell of radius  $c$ , the porosity  $\gamma$  was calculated as the relative liquid volume of the cell  $1 - \frac{b^3}{c^3}$  and the volume of the inter-cell space was neglected. For the cell structure considered in the present paper, the pore volume in the layer  $\ell < r < 1$  should be added to this magnitude, so it takes the form  $\gamma = \frac{c^3 - b^3 + \varepsilon(b^3 - a^3)}{c^3} = 1 - \frac{1}{m^3} + \varepsilon \frac{1 - \ell^3}{m^3}$ . For large values of  $\ell$  (thin porous layer), the last term can be neglected and the membrane porosity can be calculated simply as  $\gamma \approx 1 - 1/m^3$ . The dependence of the hydrodynamic permeability on  $\gamma$  defined in this manner is shown in Fig. 8 for  $\ell = 0.9$ . The plot demonstrates the dominating role of the porosity  $\gamma$  in determining hydrodynamic permeability. The curves being close to each other and the sharp increase in  $L_{11}$  observed for all BVP statements and liquid types imply a secondary role of all these conditions when the dependence of  $L_{11}$  on the membrane porosity is studied.

The obtained theoretical dependence of the membrane hydrodynamic permeability on its active porosity was compared with the experimental data of [39]. The experiment considered the flow of a water–ethanol mixture through a nanoporous membrane based on poly(1-trimethylsilyl-1-propyne) for various pressure gradients and mass fractions of the ethanol in the mixture. The membranes were developed using the tape-cast method. In the flow experiments, the mass flow rate was measured for each pressure gradient applied to the system. Then, the permeability of the membrane was calculated based on the Darcy law. The dependence of permeability on active porosity was obtained for three sets of conditions for the pressure gradient and ethanol concentration. Both these characteristics influence the ability of the membrane to conduct liquid. It is known that this type of membranes is almost impermeable for pure water and its permeability increases when the ethanol concentration in the mixture rises. The reason for this effect lies in the hydrophilization of the membrane material by the adsorbed ethanol molecules. This effect was modeled in [39] as the pore opening process and was formalized by introducing the concept of effective porosity. The latter was defined as the fraction of pores opened for the flow. The mass flow rate was evaluated on the basis of a hydrodynamic model that interpreted filtration as a flow through a set of cylindrical pipes of radii subjected to the given distribution law. Finally, the measured and the theoretical flow rates were equated and the fraction of pores filled with the liquid was calculated.

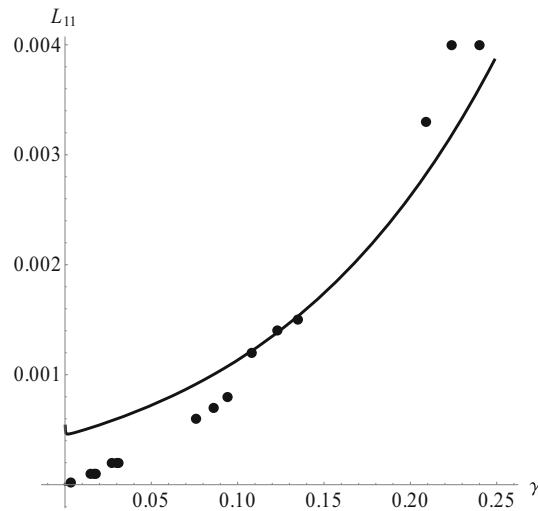


**Fig. 9** Calculated hydrodynamic permeability versus porosity  $\gamma$  (curve) and experimental data of [39] (points)

In the present study, the hydrodynamic permeability  $L_{11}$  is non-dimensional, so the experimental data should be transformed into the same non-dimensional units. Based on the definition of hydrodynamic permeability, its dimension can be represented as a squared length divided by viscosity. The characteristic length  $b$  used in relations (3) represents the order of the cell size; it was estimated using the simplest orthogonal package of the spherical solid parts of the cells, the voids between them approximated by spheres. This estimate relates the characteristic scale  $b$  to the porosity of the sample and its average pore size, which were taken from [39]. In addition, the membrane swelling and its dependence on the mixture composition were taken into account in the calculation of the average pore size, as offered in [39]. As a result, the value of  $b$  turned out to be dependent on the ethanol concentration in the mixture, apart from the sample porosity. Each experimental value was divided by the corresponding value of  $b^2$  and multiplied by the mixture viscosity. The variation in the latter with ethanol concentration was also taken into account. The obtained points and the corresponding theoretical curve are shown in Fig. 9. The plotting was done for Happel's BVP, although any other curve shown in Fig. 8 is applicable as well. The curve in Fig. 9 is plotted for the same parameters as shown in Fig. 8 except for  $\varepsilon$ , which was taken to be equal to 0.6 in order to diminish the value of hydrodynamic permeability at zero porosity. The model includes the flow through the porous core of the cell, so the calculated velocity and, consequently, the hydrodynamic permeability are nonzero even if the fraction of voids in the membrane is negligibly small ( $\gamma \rightarrow 0$ ).

As seen from Fig. 9, the presented theoretical model reasonably agrees with the experimental data. The curve represents the nature of the dependence, the main trend, the order of magnitude, and the convex direction. It overestimates hydrodynamic permeability for low porosity values for the reason specified above and underestimates its value when porosity increases. This discrepancy may be due to the fact that the method of the effective porosity evaluation in [39] used the Newtonian liquid model: it is known that the classical model usually gives higher permeability values than the micropolar model.

Two other experimental datasets were used in [31] for the verification of the cylindrical cell model. They also demonstrated good agreement with the theory developed there.

## 6 Conclusion

The study presented in this paper concludes a series of investigations devoted to the development of the cell model technique for filtration flows of micropolar fluids. It includes the most general configuration of a spherical cell which consists of a solid core, a porous shell, and a liquid envelope. Varying the thickness of these layers allows us to consider various limiting cases, namely a fully solid core ( $\ell \rightarrow 1$ ), an entirely porous core ( $\ell \rightarrow 0$ ), and a solid-porous cell ( $m \rightarrow 1$ ). Varying the porous layer parameters enables modeling of the membrane permeability within a wide range of values (from negligible to maximal, corresponding to a pure matrix without a porous coating). The introduced parameters of the permeating liquid represent a wide variety

of its properties, from classical to strongly polar. The statements of several types of BVPs were given, and their analytical solutions were obtained. The expressions for the flow velocity components were presented in a finite form, suitable for practical applications.

The hydrodynamic permeability, taken as an integral characteristic of the membrane, has a rather cumbersome analytical representation, so it was investigated in computational parametric experiments. They demonstrated a noticeable effect of the considered boundary conditions at the outer surface of the cell on the hydrodynamic permeability. A moderate variation in the hydrodynamic permeability was observed for the whole range of the micropolar parameters of the liquid,  $N$ ,  $L$ ,  $\phi$ , and the characteristics of the porous layer of the cell,  $\varepsilon$  and  $\sigma$ . The active porosity of the membrane,  $\gamma$ , had the strongest effect on its hydrodynamic permeability. The obtained dependence was compared to the experimental data, and a reasonable agreement was observed.

The interpretation of experiments remains one of the biggest challenges in membrane science. The studies of fine membrane properties continue even for commercially available membranes [40]. The presented model is aimed at the improvement in our understanding of the membrane processes. The flexibility of the model allows for its application to a wide variety of materials and liquids. The obtained analytical results are suitable for engineering research. Despite promising advantages, the theory of micropolar liquids is extremely rarely used in experiment interpretation today. This paper may serve as a step toward promoting its wider practical application.

**Acknowledgements** The present work is supported by the Russian Foundation for Basic Research (19-08-00058).

#### Compliance with ethical standards

**Conflict of interest** The author declares no conflict of interest.

#### References

- Nield, D.A., Bejan, A.: Convection in Porous Media, 3rd edn. Springer, New York (2006)
- Brinkman, H.C.: A calculation of the viscous force exerted by a flowing fluid on a dense swarm of particles. *J. Appl. Sci. Res.* **A1**, 27–34 (1947)
- Happel, J., Brenner, H.: Low Reynolds Number Hydrodynamics. Martinus Nijhoff Publishers, The Hague (1983)
- Perepelkin, P.V., Starov, V.M., Filippov, A.N.: Permeability of a suspension of porous particles. *Cellular. model. Kolloidn. Zh. - Colloid J.* **54**(2), 139–145 (1992). (in Russia)
- Vasin, S.I., Starov, V.M., Filippov, A.N.: Hydrodynamic permeability of a membrane regarded as a set of porous particles (the cellular model). *Kolloidn. Zh. - Colloid J.* **58**(3), 307–311 (1996). (in Russia)
- Vasin, S.I., Starov, V.M., Filippov, A.N.: Motion of a solid spherical particle covered with a porous layer in a liquid. *Kolloidn. Zh. - Colloid J.* **58**(3), 298–306 (1996). (in Russia)
- Vasin, S.I., Filippov, A.N.: Hydrodynamic permeability of the membrane as a system of rigid particles covered with porous layer (cell model). *Colloid J.* **66**(3), 305–309 (2004)
- Filippov, A.N., Vasin, S.I., Starov, V.M.: Mathematical modeling of the hydrodynamic permeability of a membrane built up from porous particles with a permeable shell. *Colloids Surf. A Physicochem. Eng. Asp.* **282–283**, 272–278 (2006)
- Vasin, S.I., Filippov, A.N., Starov, V.M.: Hydrodynamic permeability of membranes built up by porous shells: cell models. *Adv. Coll. Interface Sci.* **139**, 83–96 (2008)
- Vasin, S.I., Filippov, A.N.: Cell models for flows in concentrated media composed of rigid impermeable cylinders covered with a porous layer. *Colloid J.* **71**(2), 141–155 (2009)
- Vasin, S.I., Filippov, A.N.: Permeability of complex porous media. *Colloid J.* **71**(1), 31–45 (2009)
- Deo, S., Filippov, A.N., Tiwari, A., Vasin, S.I., Starov, V.M.: Hydrodynamic permeability of aggregates of porous particles with an impermeable core. *Adv. Coll. Interface Sci.* **164**(1), 21–37 (2011)
- Yadav, P.K., Tiwari, A., Deo, S., Filippov, A.N., Vasin, S.I.: Hydrodynamic permeability of membranes built up by spherical particles covered by porous shells: effect of stress jump condition. *Acta Mech.* **215**, 193–209 (2010)
- Yadav, P.K., Tiwari, A., Singh, P.: Hydrodynamic permeability of a membrane built up by spheroidal particles covered by porous layer. *Acta Mech.* **229**, 1869–1892 (2018)
- Happel, J.: Viscous flow in multiparticle system: slow motion of fluids relative to beds of spherical particles. *AIChEJ* **4**(2), 197–201 (1958)
- Happel, J.: Viscous flow relative to arrays of cylinders. *AIChEJ* **5**(2), 174–177 (1959)
- Kuwabara, S.: The forces experienced by randomly distributed parallel circular cylinders or spheres in a viscous flow at small Reynolds numbers. *J. Phys. Soc. Jpn.* **14**, 527–532 (1959)
- Mehta, G.D., Morse, T.F.: Flow through charged membranes. *J. Chem. Phys.* **63**(5), 1878–1889 (1975)
- Cunningham, E.: On the velocity of steady fall of spherical particles through fluid medium. *Proc. R. Soc. Lond.* **A83**, 357–365 (1910)
- Kvashnin, A.G.: Cell model of suspension of spherical particles. *Fluid Dyn.* **14**, 598–602 (1979)
- Sochi, T.: Non-Newtonian flow in porous media. *Polymer* **51**, 5007–5023 (2010)
- Cosserat, E., Cosserat, F.: *Theorie des Corps Deformables*. Hermann et Fils, Paris (1909)

23. Eringen, A.C.: Simple microfluids. *Int. J. Eng. Sci.* **2**, 205–217 (1964)
24. Eringen, A.C.: Theory of micropolar fluids. *J. Math. Mech.* **16**, 1–18 (1966)
25. Khanukaeva, D.Yu., Filippov, A.N.: Isothermal flows of micropolar liquids: formulation of problems and analytical solutions. *Colloid J.* **80**(1), 14–36 (2018)
26. Saad, E.I.: Cell models for micropolar flow past a viscous fluid sphere. *Meccanica* **47**, 2055–2068 (2012)
27. Prasad, M.K., Kaur, M.: Wall effects on viscous fluid spheroidal droplet in a micropolar fluid spheroidal cavity. *Eur. J. Mech. B/Fluids* **65**, 312–325 (2017)
28. Sherief, H.H., Faltas, M.S., Ashmawy, E.A., Abdel-Hameid, A.M.: Parallel and perpendicular flows of a micropolar fluid between slip cylinder and coaxial fictitious cylindrical shell in cell models. *Eur. Phys. J. Plus* **129**, 217 (2014)
29. Sherief, H.H., Faltas, M.S., Ashmawy, E.A., Nashwan, M.G.: Stokes flow of a micropolar fluid past an assemblage of spheroidal particle-in-cell models with slip. *Phys. Scr.* **9**(5), 055203 (2015)
30. Khanukaeva, D. Yu., Filippov, A.N., Yadav, P.K., Tiwari, A.: Creeping flow of micropolar fluid parallel to the axis of cylindrical cells with porous layer. *Eur. J. Mech. B/Fluids* **76**, 73–80 (2019)
31. Khanukaeva, D. Yu., Filippov, A.N., Yadav, P.K., Tiwari, A.: Creeping flow of micropolar fluid through a swarm of cylindrical cells with porous layer (membrane). *J. Mol. Liq.* **294**, 111558 (2019)
32. Eringen, A.C.: *Microcontinuum Field Theories-II: Fluent Media*. Springer, New York (2001)
33. Nowacki, W.: *Theory of Micropolar Elasticity*. Springer, Wien (1970)
34. Kamel, M.T., Roach, D., Hamdan, M.H.: On the micropolar fluid flow through porous media, In: *Mathematical Methods, System Theory and Control, Proceedings of the 11th MAMECTIS'09*, pp. 190–197. WSEAS Press, New York (2009). ISBN: 978-960-474-094-9
35. Hamdan, M.H., Kamel, M.T.: Polar fluid flow through variable-porosity, isotropic porous media. *Spec. Top. Rev. Porous Med. Int. J.* **2**(2), 145–155 (2011)
36. Lukaszewicz, G.: *Micropolar Fluids—Theory and Applications*. Birkhäuser, Basel (1999)
37. El-Sapa, S.: Settling slip velocity of a spherical particle in an unbounded micropolar fluid. *Eur. Phys. J. E* **42**, 32–39 (2019)
38. Filippov, A.N., Khanukaeva, D.Yu., Vasin, S.I., Sobolev, V.D., Starov, V.M.: Liquid flow inside a cylindrical capillary with walls covered with a porous layer (gel). *Colloid J.* **75**(2), 214–225 (2013)
39. Filippov, A.N., Ivanov, V.I., Yushkin, A.A., Volkov, V.V., Bogdanova, YuG, Dolzhikova, V.D.: Simulation of the onset of flow through a PTMSP-based polymer membrane during nanofiltration of water–methanol mixture. *Petr. Chem.* **55**(5), 347–362 (2015)
40. Duan, Q., Wang, H., Benziger, J.: Transport of liquid water through Nafion membranes. *J. Membr. Sci.* **392–393**, 88–94 (2012)